Research Article

Ibtisam Ahmed Jarih*, Abdulamir Atalla, and Alaa C. Galeb

Behavior of container berth structure under the influence of environmental and operational loads

https://doi.org/10.1515/eng-2024-0022
received February 08, 2024; accepted March 30, 2024

Abstract: Container docks, which are an essential component of the marine berth, are exposed to loads from various sources, such as self-weight, operation, and environment. In this study, four sets of combined loads to which the container berth is exposed were selected at the Um-Qaser Port in southern Iraq. The berth was constructed more than 40 years ago, which has to be verified according to latest specifications, and each set of combined loads was analyzed in three cases. In the first case, the piles were assumed to be fixed at the seabed, and in the second and third cases the piles were modeled as embedded in elastic and elasto-plastic sandy soil, respectively. The general-purpose finite-element software ABAQUS was used to model the various components to determine the maximum stresses, displacements, axial forces, shear forces, and bending moments due to dead, live, operate, berthing, mooring, waves, and seismic loads. It has been demonstrated that the impact loads of ships have a more significant impact on the structure compared to other loads. The calculated displacement when the piles are assumed to be fixed at the seabed level may be reduced by 50–94% of that calculated when the soil is modeled, meaning that assuming fixed piles yields inaccurate results, especially for deck displacements. However, this assumption was verified to yield reasonable results for shear forces at the pile head. It could also be noted that the elasto-plastic model of soil was more sensitive than the elastic model in displacement by 0.4–8% and bending moment by 0.3–34%, while it is less sensitive in axial force by 3–8%. The aim of this study is to obtain knowledge on the behavior and efficiency of container berth under the influence of different loads and the environmental conditions surrounding it.

Keywords: marine berth, berthing loads, mooring, ship impact, wave forces

1 Introduction

To assist in the loading and unloading of goods as well as the boarding and alighting of passengers and vehicles, berthing structures are designed to anchor and berth vessels. The targeted location's soil characteristics, the amount of traffic, and the surrounding environment are some of the factors that affect the planning and building of berthing structures. The majority of structures associated with ports may be broadly categorized into piles, bulkheads, pile caps, decks, fenders, and mooring fittings. Numerous studies have addressed the issue of offshore structures and ship collisions. Edvardsen *et al.* researched offshore constructions' ability to withstand impact stress from falling debris and boats in 1983 [1]. In 1983, Amdahl studied the deformation of circular tubes due to lateral impact. Using a hard plate, the lateral force was delivered parallel to the tube's axis [2]. In 1988, Wierzbicki and Suh looked at the deformation of circular tubes in response to lateral impacts. A line impact was used to apply the force to a single tube portion [3]. In 2000, Al-Jasim looked into the berthing load from an oil tanker with 330,000 DWT at 60% cargo at Khor-Al-Amaya port number 8 [4]. In 2003, Hussein investigated the three-dimensional offshore structure's dynamic response to wave loading and ship collision [5]. In 2006, Al-Shinawah studied the dynamic response of a container dock to three loading cases (water waves, ship influence, and a combination of the two). It is concluded that the case of ship impact is the worst, considering the bending moment, force, and deflection of piles, while the combination case is the worst for the deck displacements [6]. In 2012, Kadim investigated the dolphin's dynamic reaction to the effect of the ship berthing at Khor-Al-Amaya berth No. 8. The influence of fluid–structure interaction on the dynamic response was investigated by accounting for the forces of wind and waves [7]. In

* **Corresponding author: Ibtisam Ahmed Jarih**, Civil Engineering Department, University of Basrah, Basrah, Iraq, e-mail: pgs.ibtisam.ahmed@uobasrah.edu.iq
Abdulamir Atalla: Civil Engineering Department, University of Basrah, Basrah, Iraq, e-mail: abdulamir.karim@uobasrah.edu.iq
Alaa C. Galeb: Civil Engineering Department, University of Basrah, Basrah, Iraq, e-mail: Alaa.galeb@uobasrah.edu.iq

2014, Travanca and Hao examined how an offshore platform behaves dynamically when a vessel impacts it with a lot of energy. This research featured a process to enhance comparable systems [8]. In 2016, Hasan examined the dolphin structure of Um-Qaser. Additionally, he looked at how the soil properties and pile size affected the way the structure behaved under stress when the soil was thought to be elasto-plastic. The Cam-Clay soil model was used to study the Um-Qaser container terminal under the influence of ship loading. It was discovered that the elasto-plastic model's displacements are 10% higher than those of the elastic model [9]. Xie *et al.* investigated the lateral load behavior of high-piled wharf by the finite-element software – ANSYS. The numerical simulation results of pile top displacement are found to be in good agreement with those predicted using the theoretical formula [10]. Ali *et al.* assessed the behavior of the cylindrical rubber fender in response to the berthing force delivered by a moored ship with a capacity equal to 330,000 DWT [11]. Daliri and Naimi looked at ways to extend the serviceability life of the offshore jacket structure and simplify the building process. The ANSYS software was used in this work. Extreme wave loading and vessel impact load included the transient dynamic load delivered to the offshore jacket [12]. Lei *et al.* studied the seismic fragility of a large-scale PSWS located at the Port of Los Angeles Berth 100, USA, with and without considering SPI (soil–pile interaction), who showed that SPI significantly influences the seismic fragility of the PSWS. For distinct damage states, the effect of SPI on the seismic fragilities of different piles can be totally different [13]. In 2019, Ahemer studied the dynamic response of the Al-Basrah Oil Port under the effect of wave, ship impact, and seismic loads by the ABAQUS program. He reported that the response of structure under seismic load with a fixed support is less than that of structure with an embedded pile as the support [14]. De Carvalho *et al.* conducted an investigation on the forces developed on the mooring system of vessels berthed at dolphins. The vessel's displacement and their peak value were determined through stochastic and statistical theories [15]. Al-Abbas *et al.* investigated the performance of steel-tube columns filled with reactive powder concrete under axial compression with different cross sections [16]. In 2023, Cuong and The Anh presented an algorithm and developed a formula to evaluate the dynamic effect of wave loading on fixed-steel offshore structures [17]. Gjukaj *et al.* used the ABAQUS FE software to construct a three-dimensional finite-element model with the main objective of exploring how different geometric parameters impact the behavior of the extended end-plate bolted connection, which functions as a semi-rigid partial-strength beam-to-column connection [18]. Wang *et al.* studied seismic response models of two types of high-piled wharves, namely, the as-built group and the retrofit group. The study included analysis and interpretation of deck displacement, pile deformation, and pile bending moment under the EI-centro wave and the Northridge wave, with peak accelerations of 0.2 and 0.4 g, respectively [19].

This study examined the reaction of the wharf structure to combined loads by numerical simulation using the ABAQUS software; the container berth at Um-Qasr Port was used for this purpose.

2 Research methodology

The ABAQUS finite-element program was used to simulate the problem. The details of the analysis model of Um-Qaser container berth are shown in Figure 1. To do the modeling, one unit of pavement was chosen with dimensions 46 m × 25 m × 0.7 m containing 40 piles arranged in eight columns with a distance of 6 m and five lines in a row with a distance of 5.5 m. The concrete deck slab, steel-beam section, and soil were modeled using eight-node brick elements, so that each node has three degrees of freedom representing the translation motion in three global coordinates. The piles (steel pipes) were modeled using a three-dimensional four-node shell (S4R) structure. Figure 2 shows the three-dimensional modeling of the structure with soil dimensions.

Appropriate establishment of the soil mass dimensions is necessary to minimize the impact of borders on the outcomes. Boundary condition: it includes all soil domains that are regarded as fixed, with the exception of the top, which is regarded as free. The length of the piles to the soil boundary's borders is equal to 10D (pile diameter), whereas the distance from the ends of the piles to the bottom of the soil boundary equals to 10D.

Using the Mohr–Coulomb model, nonlinear behavior is modeled. One way to express the Coulomb criteria of failure is the following expression, which was adapted from Naylor and Pande [20–22]:

$$|\tau| \le \sigma n \tan \phi + c, \tag{1}$$

where τ is the shear stress, σn is the normal effective stress, c is the cohesion, and ϕ is the internal angle of shearing friction.

Full bond is used to represent the link between soil and piles. The value of the damping ratio used in the analysis of the present study is equal to 0.05.

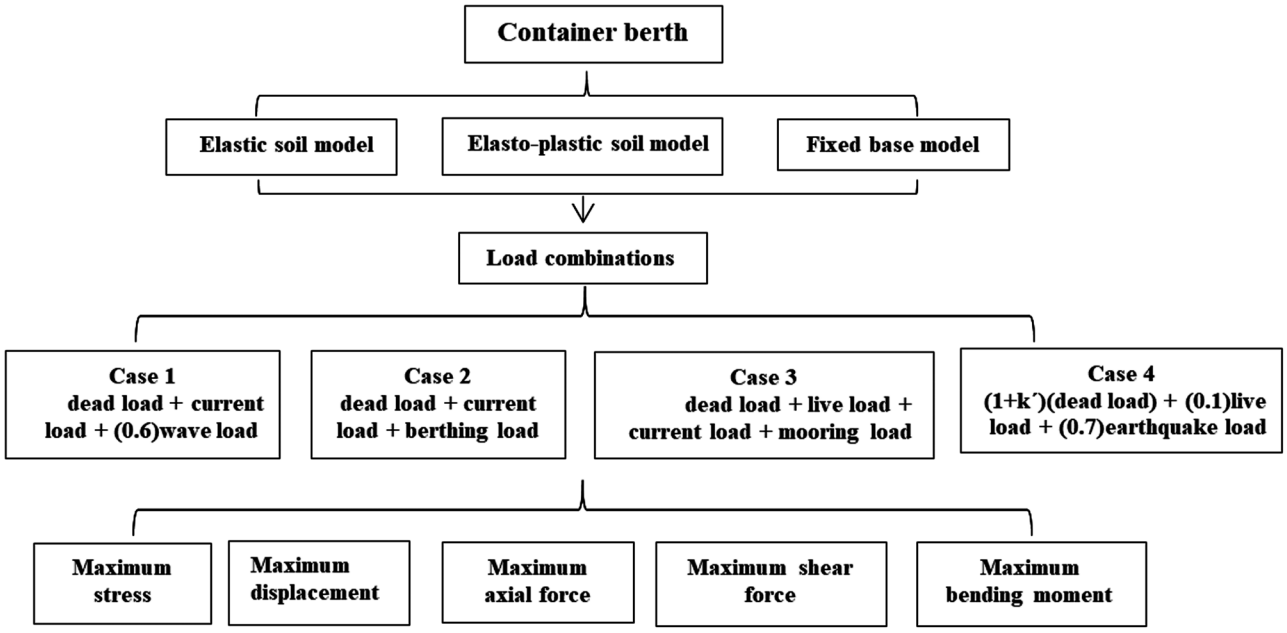

Figure 1: Flowchart illustrating the research.

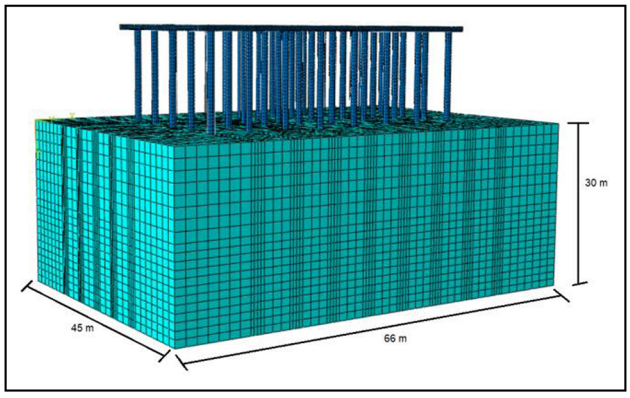

Figure 2: 3D modeling of the Um-Qaser container terminal with Abaqus.

The berth structure is subjected to four load combinations:

Case (1): [dead load + current load + (0.6) wave load]

Case (2): [dead load + current load + berthing load]

Case (3): [dead load + live load + current load + mooring load]

Case (4): [(1 + k')(dead load) + (0.1) live load + (0.7) earthquake load],

where k' = 0.35 (peak ground acceleration) [23].

Dead loads include the self-weight of a structure calculated by the program and the roof load (compacted sand and asphalt paving). The live load resulted from shedding container load, traffic, and crane load [24]. The ship is generally berthing parallel to the current. On piles parallel to the direction of the water current, the intensity of pressure shall be calculated from the following equation:

$$F_C = C_c \times A_c \times \gamma V^2/2g, \tag{2}$$

where F_C is the current force, γ is the unit weight of water (1.025 t/m^3), V is the velocity of current (0.3 m/s), C_c is 0.22 for the circular pile, and A_c is the area of the ship's underwater part projected onto a plane perpendicular to the direction of current (m^2).

Morison's equation was used to calculate the wave. Originally designed to calculate the hydrodynamic forces operating at a right angle to the steady flow on a cylinder, this equation is expressed as follows:

$$dF_T = \left(\rho\pi\frac{D^2}{4}C_m a + \rho C_d u|u|\right)dz. \tag{3}$$

Here, ρ is the water density, D is the cylinder diameter, and C_m and C_d are, respectively, the inertia and drag coefficients, assuming that the wave force is acting on the vertical distance (dz) of the cylinder due to the velocity (u) and acceleration (a) of water particles [25]. The Airy theory was used to calculate the wave speed. Table 1 includes the details of properties of seawater collected from the information related to the Arabian Gulf for the past 100 years showing the maximum wave load [26].

Based on the vessel's dead weight tonnage (50,000), the reaction force on the fender, which corresponds to the above tonnage, is approximately 200 t [24]. Mooring point

Table 1: Sea water characteristics [28]

Item	Symbol	Value	Unit
Water depth	*d*	9	M
Water density	*y*	1,025	kg/m^3
Water viscosity	*V*	1.2×10^{-6}	m^2/s
Gravity acceleration	*g*	9.81	m^2/s
Wave height	*h*	2	M
Wavelength	*L*	7.5	M
Wave period	*T*	4	s

loads general cargo vessels and bulk carriers, the value of which was based on the table from Maritime works, Code of practice for design of fendering and mooring systems [27]. The earthquake at Ali Al-Gharbi, Maysan, Iraq, shown in Figure 3 is used to simulate the seismic load and acceleration time. The time history method is used in the ABAQUS program for berth port analysis.

Figures 4–7 show the applied loads on the berth structure for the four cases of combination loads. Table 2 includes all structural parts along with their dimensions, and Table 3 includes all material properties used in the current study.

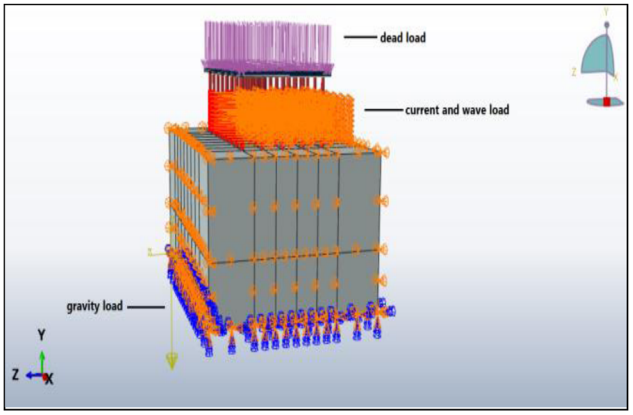

Figure 4: Case (1) load combinations.

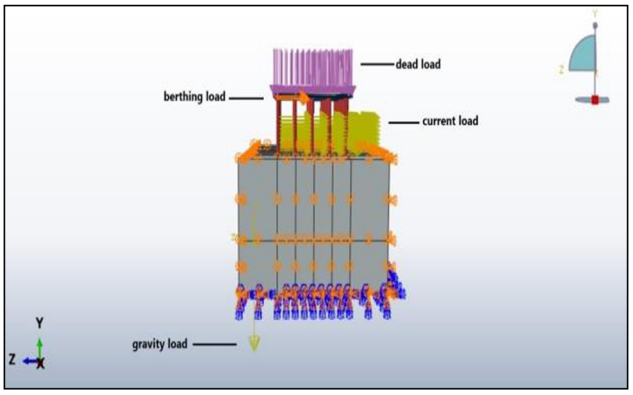

Figure 5: Case (2) load combinations.

3 Results and discussion

The behavior of contact junctions between the enclosing soil and the structural element has a considerable impact on the response of structure–foundation systems to static or dynamic loads. These junctions represent the interface between the response of the soil – structure which transmits the load and the deformations. Tables 4–7 contain the highest values of the analysis results for the Umm Qasr container berth under the influence of four cases of combined loads and three types of pile stabilization. The values of these results indicate that the fixed state of the pile tip at the seabed is less responsive than the state supported by soil. Also, the second load case (berthing of the ship) has more impact on the structure than the other load cases.

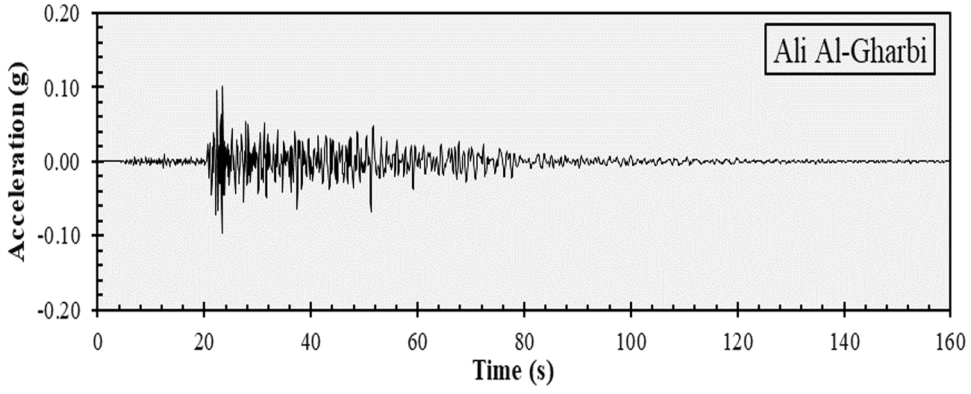

Figure 3: Ali Al-Gharbi earthquake.

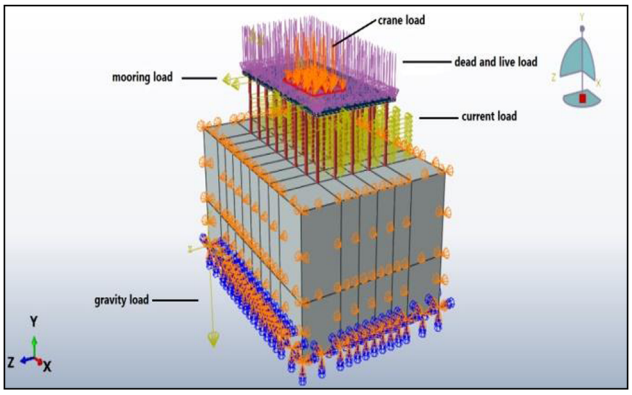

Figure 6: Case (3) load combinations.

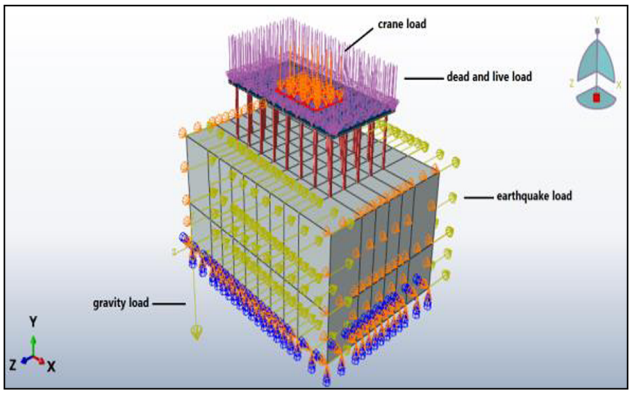

Figure 7: Case (4) load combinations.

Figure 8 shows the state of maximum displacement of the berth deck for the first loading case; deformation is noted if the pile is embedded in sand soil to a depth of 18 m, and the structure is more response; we can also notice that there is a similarity in the deformation of the berth deck in the cases of elastic and elasto-plastic soil, while the calculated displacement when the piles are assumed to be fixed at the sea bed level may be reduced by about 94% of those calculated when the soil is modeled. At the beginning of the loading, the displacement increases upward and then takes a horizontal path due to vertical loads and lateral loads. Figure 9 shows the state of total deformation of the berth deck for the second loading case,

Table 3: Details of the material

Material	Elastic modulus (MPa)	Poisson's ratio	Cohesion (kPa)	Density (kg/m^3)
Steel	200,000	0.3	—	7,800
Concrete	25,000	0.2	—	2,400
Soil	57	0.35	5	2,000

Table 4: Maximum result of whole structure under combination load case (1) (ASD)

Case	Item	Pile embedded in soil		Fixed base
		Elastic soil	Elasto-plastic soil	
(1)	Maximum stress (MPa)	79.3	76.83	46.86
	Maximum displacement (mm)	72.4	72.89	4.6
	Maximum axial force (kN)	3,179	3,082	1,873
	Maximum shear force (kN)	54.9	58	35
	Maximum bending moment (kN m)	157.6	167	107

Table 5: Maximum result of whole structure under combination load case (2) (ASD)

Case	Item	Pile embedded in soil		Fixed base
		Elastic soil	Elasto-plastic soil	
(2)	Maximum stress (MPa)	169.5	216.4	105
	Maximum displacement (mm)	141.7	150.8	75.7
	Maximum axial force (kN)	3,262	3,084	1,931
	Maximum shear force (kN)	1,527	1,558	1,552
	Maximum bending moment (kN m)	1,655	1,668	1,532

Table 2: Details of the berth structure

Element	Diameter (m)	Length (m)	Width (m)	Thickness (m)
Pile	0.914	32	—	0.014
Deck	—	46	25	0.7
Soil	—	66	45	30

Table 6: Maximum result of whole structure under combination load case (3) (ASD)

Case	Item	Pile embedded in soil		Fixed base
		Elastic soil	Elasto-plastic soil	
(3)	Maximum stress (MPa)	111	105	92.03
	Maximum displacement (mm)	93.3	93.6	25.9
	Maximum axial force (kN)	4,165	4,021	3,684
	Maximum shear force (kN)	355	420	476.4
	Maximum bending moment (kN m)	728.5	731	566

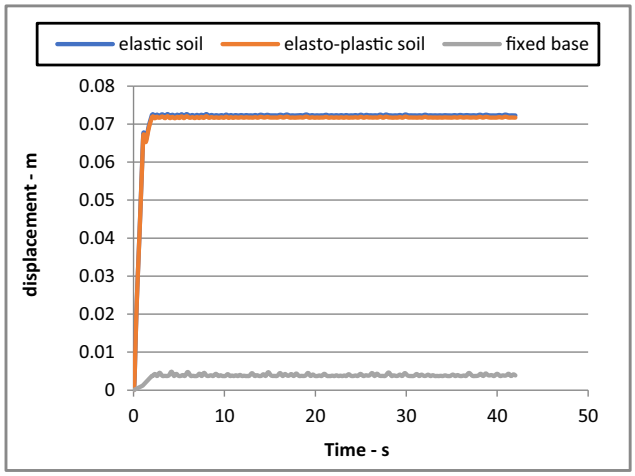

Figure 8: Deck displacement under load case (1).

Table 7: Maximum result of whole structure under combination load case (4) (ASD)

Case	Item	Pile embedded in soil		Fixed base
		Elastic soil	Elasto-plastic soil	
(4)	Maximum stress (MPa)	100.6	95	56.43
	Maximum displacement (mm)	87.6	94.5	38.6
	Maximum axial force (kN)	3,992	3,739	2,264
	Maximum shear force (kN)	366	348	88
	Maximum bending moment (kN m)	601	807	489

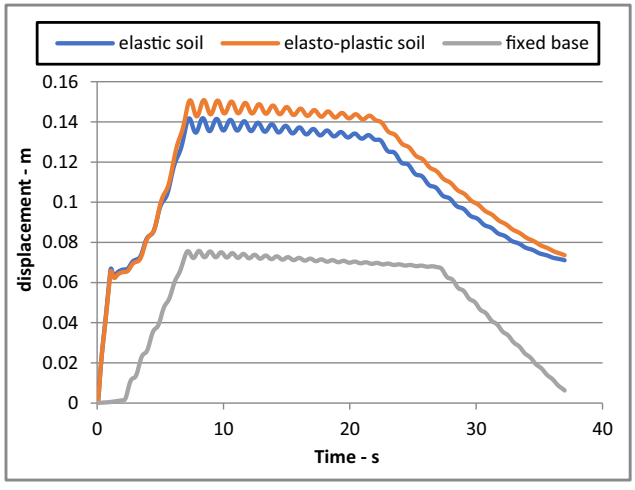

Figure 9: Deck displacement under load case (2).

which is the dead load, the current load, and the berthing load. This state of loading caused a greater deformation than the first loading state, as we see from the curve that the deformation increases at the stage of applying the ship's berthing load. We also notice that the fixed state of the tip of the pile has less deformation about 50% than the state embedded in the soil. The response of the structure to deformation in soil with elasto-plastic behavior is greater than the response to deformation in soil with elastic behavior by an amount of 6%. Hasan [9] discovered that the elasto-plastic model's displacements are 10% higher than those of the elastic model. Figure 10 shows the state of total deformation of the berth deck for the third loading case, which is the dead load, the current load, and the mooring load. This state of loading results in less deformation of the structure than in the previous loading state. We notice that the displacement is identical to the loading time for both soil conditions, while the fixed state (without soil) is less responsive by 73%. Figure 11 shows the deformation resulting from the fourth loading case. Increase the response of the structure under seismic load for the situation of soil support due to the displacement in the upper part of the soil.

The response of the structure to deformation in soil with elasto-plastic behavior is greater than the response to deformation in soil with elastic behavior by 8%. The response of the pavement surface to deformation is less than 60% when the tip of the pile is stationary at the soil surface.

Because of the displacement in the top soil, the structure responds more and more to the soil support condition, which causes piles to be fixed at a distance from the sea level. When the pile length increases to the fixation position, the pile's flexibility increases. According to the direction of the seismic force, the separation of the soil from the pile has more of an impact on that side of the pile than the

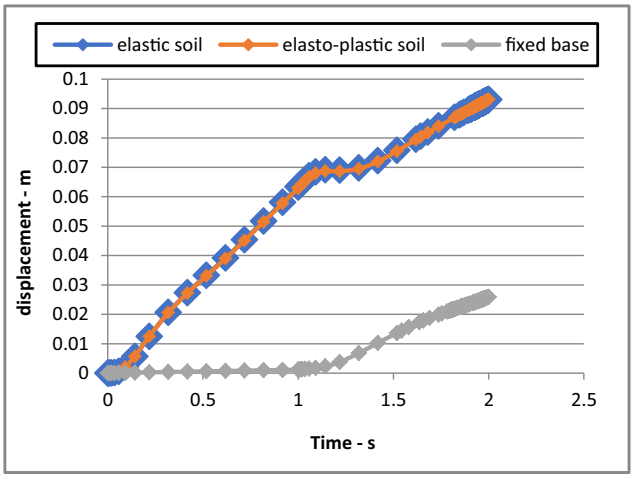

Figure 10: Deck displacement under load case (3).

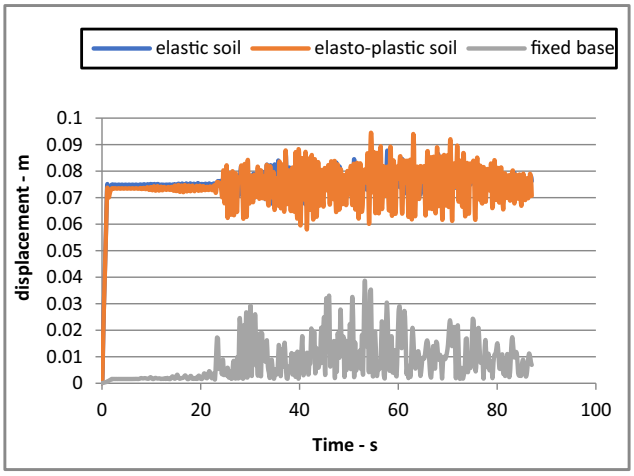

Figure 11: Deck displacement under load case (4).

other since it applies more force to the structure. When this ratio approaches one unit, it has a greater impact on the structure's response than when it is closer to the natural frequency of the structure [29,30].

Per this rule, there is a chance that the natural frequency of a structure that takes soil into consideration will be closest to the frequency of the applied load, whereas the natural frequency of a structure that has a fixed support may be greater than the frequency of the applied load. The response of a structure supported by soil is more influenced by all these factors than that of a structure with a fixed support.

Figures 12–15 show the distribution of lateral displacement along with a pile embedded in sandy soil at two states elastic and elasto-plastic, and the other state when the pile is fixed at the sea bed for four combination loading cases.

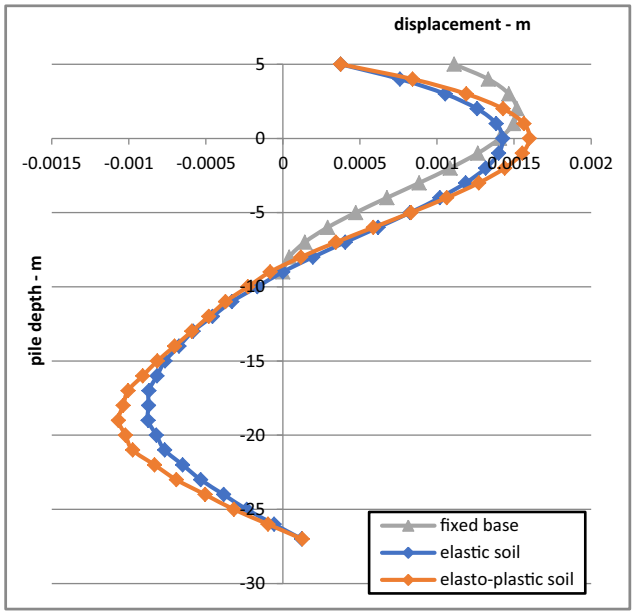

Figure 12: Pile displacement under load case (1).

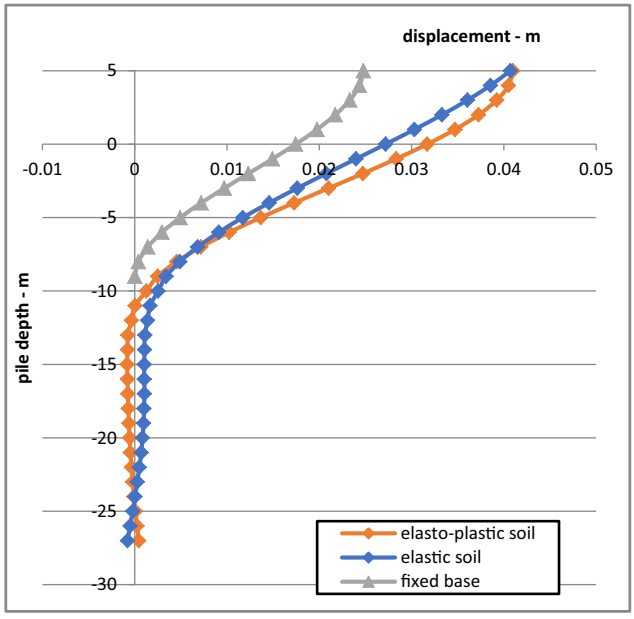

Figure 13: Pile displacement under load case (2).

As can be seen from the figure, the first loading case causes less deformation along the pile's length than the other loading cases. The pile's maximum displacement is 1.5 mm at the zero point, or the water's surface level, and it then gradually decreases until the pile's head, where this deformation is caused by the wave load and the current load applied to the pile. In the first loading case, the deformation starts at the tip of the pile, which then increases in the

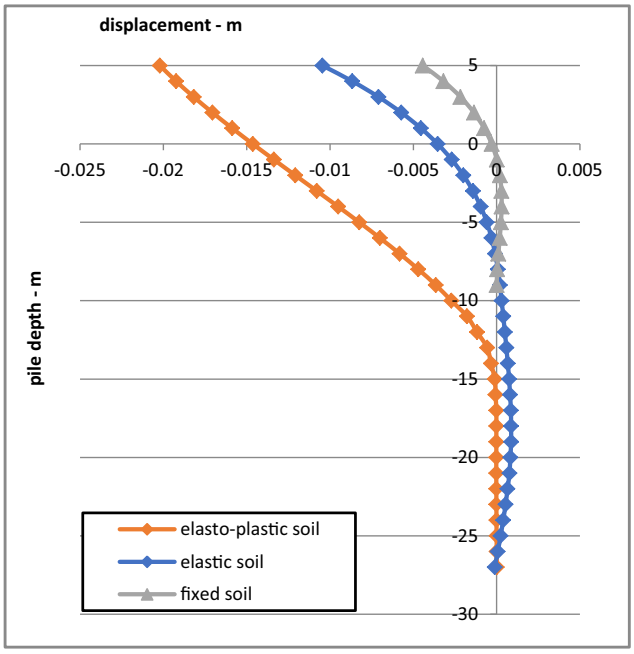

Figure 14: Pile displacement under load case (3).

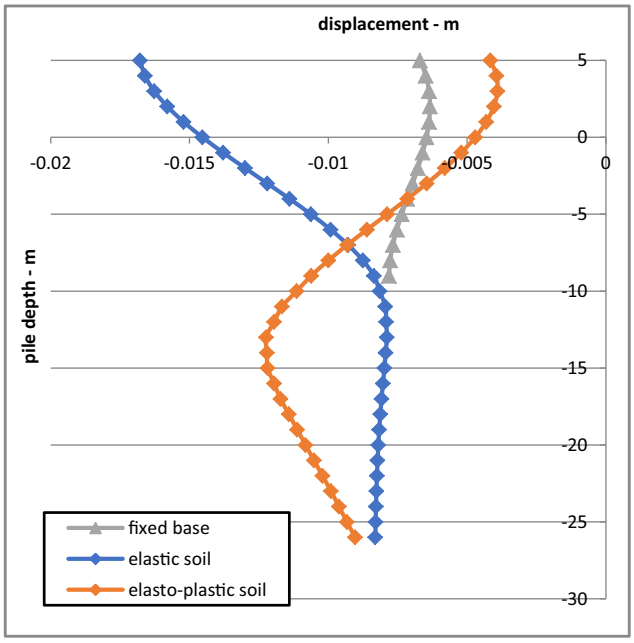

Figure 15: Pile displacement under load case (4).

middle part embedded in the soil, then returns and decreases until the surface of the soil becomes zero, then increases in the opposite direction, reaching the highest deformation at the surface of the water, after which it gradually decreases until the head of the pile. This form of deformation in the pile is due to the load applied to it from the wave and current together, it starts from the surface of the soil up to the height

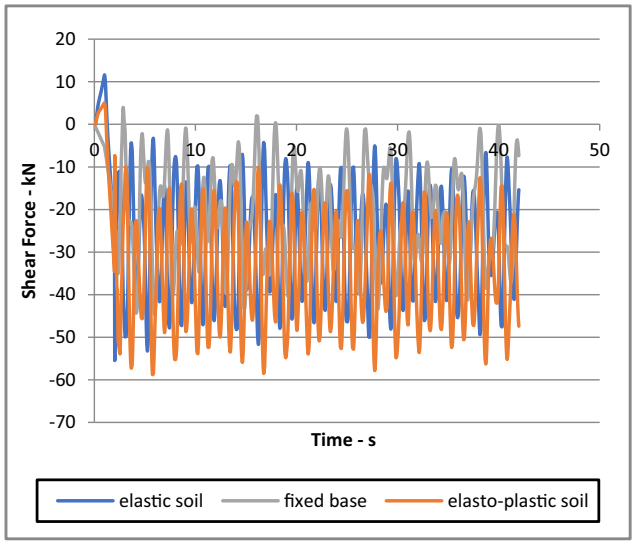

Figure 16: Shear force at the pile head under load case (1).

of the wave above the surface of the water. From the diagrams, we can notice that the highest deformation of the pile occurred in the second loading case, where the highest value was reached at the head of the pile 40.7 mm for both cases of embedding in the soil, while the fixed case of the base of the pile had the least deformation of them of 24.7 mm. The deformation of the pile fixed at the seabed is 65% less than that of the pile immersed in the soil in the second case of loading. Then coming to the third loading case, the highest deformation value was reached at 20 mm for the pile embedded in elasto-plastic soil, while in the case of elastic soil and the fixed case the deformation for pile head was 10 and 4 mm, respectively. In the fourth loading case, the highest lateral displacement of the pile head reached is 16.7 mm. From the figures of deformation of the pile, it becomes clear to us that the type and location of the load application have a significant impact on the shape of the deformation along the length of the pile. It can be noted that the deformation in the second and third loading cases, where the load is applied to the surface, we see that the deformation in the pile starts from the surface of the soil and increases toward the head of the pile. As for the part embedded in the soil, the deformation is low. As for the deformation in the pile for the fourth loading case, we notice that it starts from the tip of the pile and increases toward the middle of the part embedded in the soil, then gradually decreases at the surface of the soil, then increases in the opposite direction until the head of the pile. The deformation of the embedded part of the pile is a result of the vibration movement of the soil due to the earthquake load applied to it.

Figures 16–19 show the maximum shear forces caused by applying four cases of combined loads. Each case of

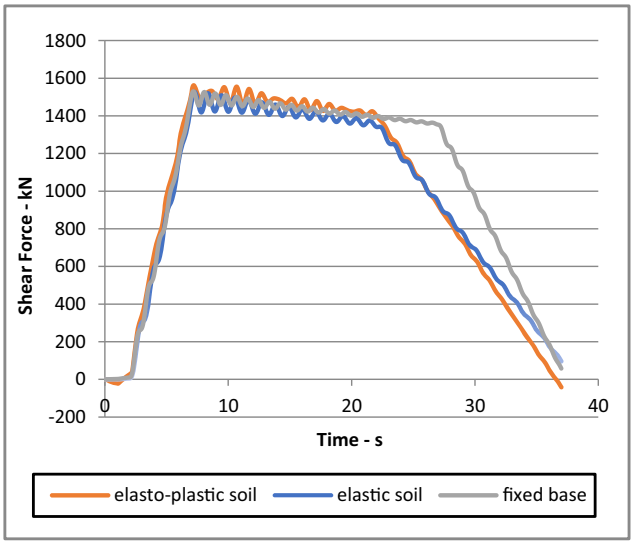

Figure 17: Shear force at the pile head under load case (2).

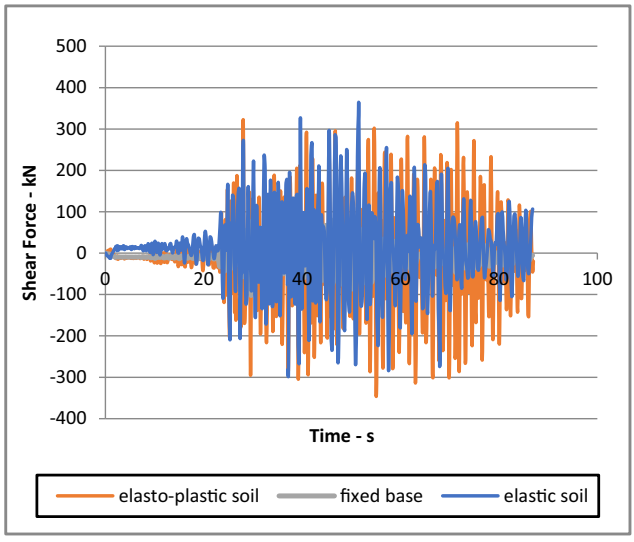

Figure 19: Shear force at the pile head under load case (4).

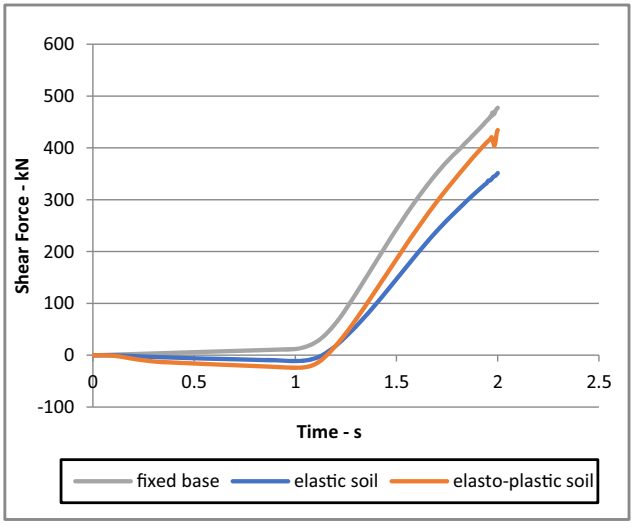

Figure 18: Shear force at the pile head under load case (3).

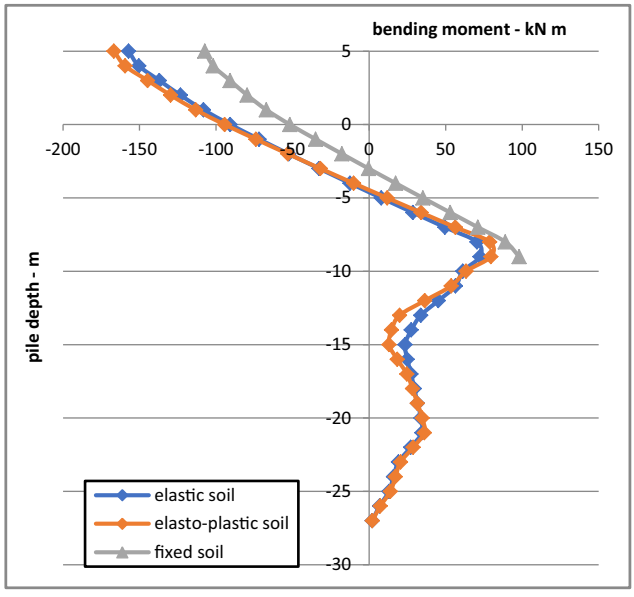

Figure 20: Bending moment under load case (1).

loading is applied to the three cases of pile fixation. The maximum shear at the first loading case is 58 kN, which occurred for the case of piles embedded in elasto-plastic soil. The shear force is found to decrease by about 5% for elasto-plastic soil modeling compared to the elastic one and decreased by about 40% for the fixed base model. The largest shear force for the second loading case is 1,558 kN, which occurred at the pile head when the piles are embedded in elasto-plastic soil. This value decreased by about 0.38% at the pile fixed base and about 2% for piles embedded in elastic soil. For the third loading case, the largest value of the shear force of 476.4 kN occurred when the case of fixed piles on the seabed, and this value is greater than about 13% from the case of the pile embedded in elasto-plastic soil and greater than by 34% from the case of the elastic soil. In the fourth case of loading, the highest response occurred in the case of pile embedded in elastic soil, where its value reached 366 kN, which is greater than the case of the pile embedded in elasto-plastic soil by about 5% and greater than that from the fixed state by four times.

The bending moment along the pile length is shown in Figures 20–23. The maximum bending moment for all cases

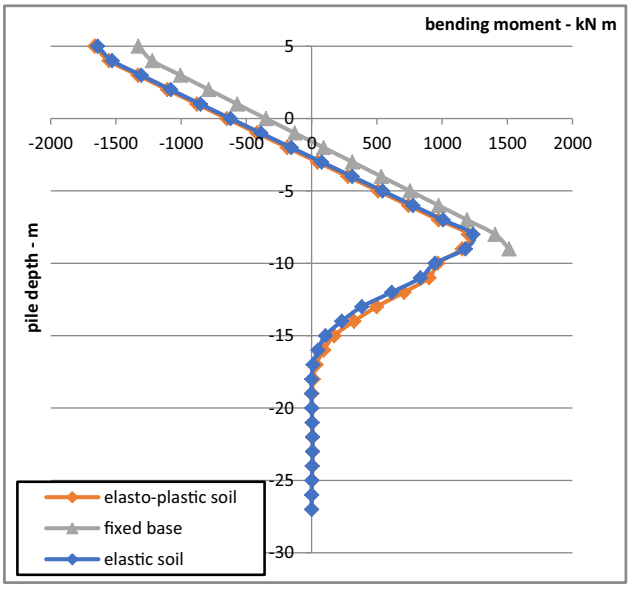

Figure 21: Bending moment under load case (2).

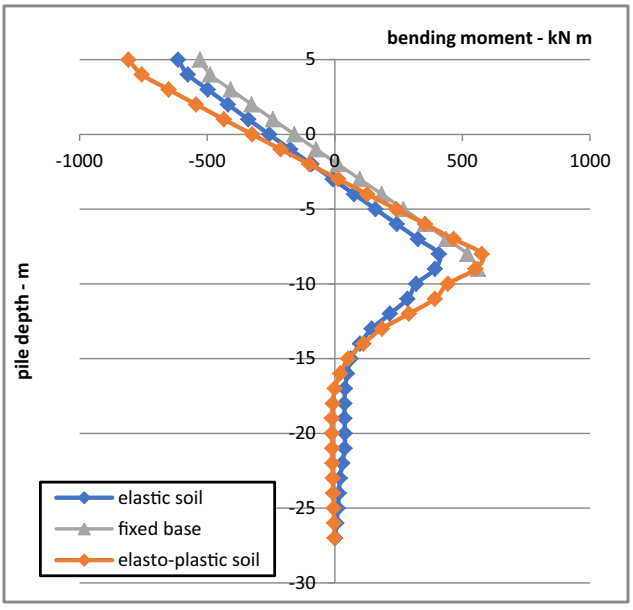

Figure 23: Bending moment under load case (4).

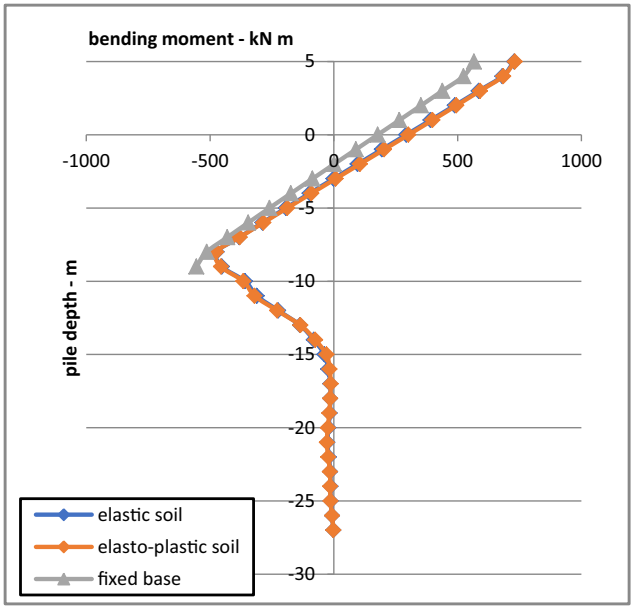

Figure 22: Bending moment under load case (3).

occurred at the pile head. The structure is more sensitive to the bending moment for the elasto-plastic soil model. The largest value of bending moment occurred in the third case of loading. The bending of the pile begins to increase at a distance of one-third of depth from the soil surface and continues to increase until it reaches a third of its depth in the water, after which it decreases to reach zero at the first third of the water depth and then increases and reaches its highest value at the head of the pile.

For the first load case, the bending moment is 167 kN m in elasto-plastic soil; this value decreases by 6% in the elastic model and by 56% in the case of the fixed pile model. For the second load case, the maximum bending moment is 1,668 kN m in the elasto-plastic model, and this value decreases by 0.8% in the elastic model and by 9% in the fixed base model. Figure 22 shows the maximum bending moment for the third loading case, which is 731 kN m at the pile head in the elasto-plastic model. We also notice that the bending moment values are identical across the length of the pile for the two cases of elastic soil and elasto-plastic soil, while the fixed case is less by 29% at the pile head. Figure 23 shows the bending moment of the pile under the influence of the fourth loading condition, where the maximum bending moment of 807 kN m was reached when the pile was embedded in elasto-plastic soil, and this value decreased in the elastic soil case and the fixed case by 34 and 65%, respectively.

4 Conclusions

The study dealt with the analysis of the container berth in the Um-Qaser Port under the effect of operation and environmental loads. The structure was analyzed for three states for each loading condition – piles embedded in elastic soil, piles embedded in elasto-plastic soil, and piles fixed at the seabed level.

The following conclusions can be drawn from the present work:

1. Considering the various load combination cases of structures is very important to identifying the loading state that mostly affects the behavior of the structure. In the present work, the second loading (berthing of ship) state is found to be most critical for the structures.
2. The elasto-plastic model of soil is more sensitive than the elastic model by 0.4–8% in the case of displacement and by 0.3–34% for bending moment, while it is less sensitive by 3–8% in the case of axial force.
3. It was found that assuming fixed ends of piles at the sea bed level may reduce the maximum displacement by about 94, 50, 73, and 60% for the wave, berthing, mooring, and seismic loading cases, respectively.
4. Deck displacement is a reflection of the deck's structural behavior under different loading conditions.
5. When designing a pile immersed in the soil, displacement, shear force, and bending moment should all be taken into account as they represent the actual behavior of the pile under different conditions of loading.

Funding information: Authors state no funding involved.

Author contributions: All authors have accepted responsibility for the entire content of this manuscript and consented to its submission to the journal, reviewed all the results and approved the final version of the manuscript. IAJ, AA and ACG contributed to the design and implementation of the research, to the analysis of the results and to the writing of the manuscript.

Conflict of interest: The authors state no conflict of interest.

Data availability statement: Most datasets generated and analyzed in this study are provided in this manuscript. The other datasets are available on reasonable request from the corresponding author with the attached information.

References

[1] Edvardsen G, Lereim J, Torset OP. Evaluation of jacket substructures subjected to impact loads from vessels and dropped objects. Offshore Struct Eng. 1984;5:460.
[2] Amdahl J. Energy absorption in ship-platform impacts. Division of marine structures. Trondheim, Norway: University of Trondheim; 1983 Sep. Report No. UR-83-34.
[3] Wierzbicki T, Suh MS. Indentation of tubes under combined loading. Int J Mech Sci. 1988;30(3–4):229–48.
[4] Al-Jasim S. Dynamic analysis of offshore template structures with soil-structure interaction. Ph.D. thesis. University of Basrah; 2000 Mar.
[5] Hussain HA. Dynamic analysis of offshore structures using finite element method. M.Sc. thesis. Engineering College Basrah University; 2003.
[6] AL-Shinawah AA. Dynamic analysis of um-qaser container terminal (case study). M.Sc. thesis. Basrah University; 2006.
[7] Kadim JA. Dynamic analysis of offshore steel structures using finite element method. Ph.D. thesis. University of Basrah; 2013.
[8] Travanca J, Hao H. Dynamics of steel offshore platforms under ship impact. Appl Ocean Res. 2014;47:352–72.
[9] Hasan A. Dynamic analysis of steel offshore structures considering the effect of soil-structure interaction. PhD thesis. University of Basrah; 2016.
[10] Xie Y, Liu C, Gao S, Tang J, Chen Y. Lateral load bearing capacity of offshore high-piled wharf with batter piles. Ocean Eng. 2017;142:377–87.
[11] Ali AM, Essa MJ, Hassan AQ, Evaluate the cylindrical rubber fender response under dynamic load. In: Seventh international conference on advances in Civil and Structural Engineering-CSE; 2017.
[12] Daliri AK, Naimi S. Transient dynamic analysis of the high-specific-strength steel jacket with extreme wave and vessel impact load. Acta Scientiarum Technol. 2018;40:496–505.
[13] Lei S, Wan H-P, Dong Y, Frangopol DM, Ling X-Z. Seismic fragility assessment of large-scale pile-supported wharf structures considering soil-pile interaction. Eng Struct. 2019;186:270–81.
[14] Ahemer AH. Dynamic analysis of oil offshore structures. PhD thesis. Engineering College University of Basrah; 2019.
[15] De Carvalho A, van LB, Campello E, Franzini GR, Skaf KJ. An assessment of mooring systems' forces of ships berthed at dolphins. Ocean Eng. 2022;253:111090.
[16] Al-Abbas B, Abdul Rasoul ZM, Hasan D, Rasheed S. Experimental study on ultimate strength of steel tube column filled with reactive powder concrete. Civ Eng J. 2023;9(6):1344–55.
[17] Cuong DQ, The Anh B. Assessment of dynamic effects of wave loads in fatigue analysis for fixed steel offshore structures. Civ Eng J. 2023;9(2):465–82.
[18] Gjukaj A, Salihu F, Ali M, Cvetanovski P. Numerical behavior of extended end-plate bolted connection under monotonic loading. HighTech Innov J. 2023;4:294–308.
[19] Wang Y, Li Y, Zhuang N, Chen H, Li K. Numerical seismic analysis of high-piled wharf strengthened with CFRP. Ocean Eng. 2023;287:115703.
[20] Naylor DJ, Pande GN. Finite elements in geotechnical engineering. Swansea, U. K.(SW/75): Pineridge Press Ltd; 1981.
[21] Mohammed A, Mahmood W. Statistical variations and new correlation models to predict the mechanical behavior and ultimate shear strength of gypsum rock. Open Eng. 2018;8(1):213–26.
[22] Ben-Dor G, Dubinsky A, Elperin T. Engineering models of high speed penetration into geological shields. Open Eng. 2014;4(1):1–19.
[23] George OL, Joseph EG, Edwin HO. SES, DAF, Michael M. Design: Piers and Wharves Unified Facilities Criteria (UFC). U.S. Army Corps of Engineers UFC; 2017.
[24] PIANC. Guidelines for the design of fender systems. Report of Working Group 33 of the Maritime Navigation Commission; 2002.
[25] Mukhopadhyay M, Sinha SK. Modelling of a fixed offshore tower in dynamic analysis. Ocean Eng. 1988;15(6):611–32.
[26] South Oil Company. Unpublished report on the structural analysis for Berth No. 8 of Khor Al-Amaya Oil Terminal. Basrah; 2007.

[27] Soetomo K. Maritime Works. Code of practice for design of fendering and mooring systems. Part 4: BS 6349-4-2014.
[28] The General Company for Ports of Iraq. Marine Testing Department; 2008.
[29] Paz M. Structural dynamic theory and computations. 2nd edn. New York: Van Nostrand Reinhold Company; 1985.
[30] Ray WC, Joseph P. Dynamic of structures, computers & structures. 3rd edn. Berkeley, CA, USA: University Ave, Berkeley USA; 2003.